International Journal of Ambient Energy

ISSN: 0143-0750 (Print) 2162-8246 (Online) Journal homepage: https://www.tandfonline.com/loi/taen20

# Influence of spent air confinement on pressure distribution over a flat plate impinged by an array of jets

Naveen G. Patil, M. Adimurthy, Vadiraj V. Katti, Mohemmedtayab A. Mujawar & S. A. Biradar

**To cite this article:** Naveen G. Patil, M. Adimurthy, Vadiraj V. Katti, Mohemmedtayab A. Mujawar & S. A. Biradar (2020): Influence of spent air confinement on pressure distribution over a flat plate impinged by an array of jets, International Journal of Ambient Energy, DOI: 10.1080/01430750.2020.1752798

**To link to this article:** https://doi.org/10.1080/01430750.2020.1752798

Accepted author version posted online: 08 Apr 2020.

**Publisher:** Taylor & Francis & Informa UK Limited, trading as Taylor & Francis Group
**Journal:** *International Journal of Ambient Energy*
**DOI:** 10.1080/01430750.2020.1752798



# Influence of spent air confinement on pressure distribution over a flat plate impinged by an array of jets

Naveen G. Patil[1*], M. Adimurthy[2] , Vadiraj V. Katti [3] , Mohemmedtayab A. Mujawar[4], S. A. Biradar[5]
[1] Teaching cum Research Assistant School of Mechanical Engineering, Vellore Institute of Technology, Vellore, India.
[2, 4, 5]Department of Mechanical Engineering, BLDEA's Vachana Pitamaha Dr. P G Halakatti College of Engineering and Tech. Vijayapura, Karnataka, India.
[3] Department of Mechanical Engineering, KLS Vishwanatharao Deshpande Rural Institute of Tech Haliyal, Karnataka, India
1* Corresponding authour:naveengpatil34@gmail.com

**ABSTRACT**

The paper deals with an experimental study carried out to determine the effect of spent air confinement on the wall-static pressure distribution (Cp) over a flat plate normal to a single row of impinging air jets. The jet after impingement is constrained to exit from one side, two opposite sides and all sides. The parameters used in the study are jet Reynolds number (Re = 10000), dimensionless nozzle-exit to target-plate spacing (z/d = 1, 2, and 3), stream-wise jet-to-jet spacing (s/d = 2 and 4), and dimensionless length of the jets (l/d = 1.0). The flat target plate is mounted on a 2D traverse table which also facilitates setting up the nozzle-exit to target-plate spacing. The pressure distribution is measured in the stream-wise direction by using a single column manometer. The cross-flow effect is found to be maximum when the spent jet is free to exit from one side only.

Keywords: confinement effect, multiple jets, streamwise pitch, spanwise pitch, wall Corresponding pressure coefficient.

## 1. INTRODUCTION

Jet impingement is a high-performance technique for forced-convection drying, heating, and cooling of surfaces. Over the past few decades, the impinging jet technology has established itself as arguably the most efficient heat transfer enhancement technique in comparison to other single-phase heat transfer configurations, and subsequently, this technology is used in myriads of industrial applications. Few of its applications being: drying of papers and textiles; the cooling of various gas turbine combustor walls; glass tempering; annealing of metals; the freezing of tissue in cryosurgery; and the cooling of electronic components, particularly for applications like the gas turbine blade cooling where heat flux is very high. Impingement cooling is highly appreciated due to its inherent characteristics of a high heat transfer rate. This kind of impinging flow device provides short flow paths and a relatively high rate of cooling for relatively small surface areas and provides localized cooling and heating.

Multi-jet system is made up of individual single jets, subsequently, multiple jets have the same jet structure or jet flow regions as the single jets. However, the multi-jet system differs from the single jet system in the following two ways: Firstly, the interference between the adjacent jets can occur before impingement on the surface Katti and Prabhu[1]. This is usually seen for smaller jet-to-jet spacing and/or when the nozzle exit to target plate spacing is high. Secondly, the collision of wall jets on the target surface after the impingement of jets as they move out in the radial direction resulting in static pressure rise at the point of collision. This interaction is possible for smaller jet-to-jet spacing and/or when the nozzle exit to target plate spacing is small, but when the jet velocity is higher. Also, another important occurrence in the multi-jet system is the presence of cross-flow, which is the flow of fluid normal to that of the impinging jets. The cross-flow can be externally induced into the system (initial cross-flow) or it can be due to the flow of accumulated spent air. The cross-flow may be in all directions, two opposite directions or just one direction. Because of these complications, the data obtained for the single jet cannot be scaled up to use for the designing of the multi-jet system. Therefore, the current study is to explore how different amount of spent air confinement affects the pressure distribution over a flat plate. Wolf et al. [2] studied the effect of the impinging jet arrays for drying of the pressed cake to determine the overall heat transfer coefficient of the system. Chang et al. [3] Experimented over the cooling of the electronic chipset by using impinging jets as well as a dimpled surface. They found that the Nusselt number will indicate that increasing the heat transfer rate. The experimental investigation from the cooling hot surface was carried out by Karwa [4] using an array of jets underwater medium. The cooling can increases when the arrays of jet increase. The experimental investigation of forced convection cooling from 3 x 3 square electronic chips using FC-72 was carried out by Wadsworth and Mudawar [5]. They observed that rectangular jets maintain nearly isothermal conditions at the chip surface, and the chip-cooling rate was independent of channel height whereas the average Nusselt number was strongly dependent on jet velocity and jet width. The experimental studies for the cooling of protruding discrete heat sources mounted at different positions on a substrate board using air as the working medium was carried out by Hotta et al [6]. The study confirms the effect of surface radiation, which reduces the temperature of electronic components by as much as 12%. Casano and Piva [7] pointed out that, internal heat removal from electronic devices is the foremost problem or else it leads to immediate failure. Some of the foremost experimental work on impinging jets is reported by Gardon and Cobonpue [8], Gardon and Akfirat [9] and Viskanta [10] providing a comprehensive review of the same. Colucci and Viskanta [11] investigated the influence of nozzle geometry on heat transfer distribution to a confined impinging air jet. The experimental parameters were: $z/d$ = 0.25 to 6.0 and $Re$ = 10000 to 50000. They reported that for all the nozzles under consideration, the $C_p$ is independent of Reynolds number, nonetheless, it is influenced by $z/d$. They also reported that at lower z/d's like $z/d$ = 0.25, the wall static pressure becomes sub-atmospheric and observed that: at even lower $z/d$'s ($z/d$ < 0.25) there exists a relatively larger and stronger region of sub-atmospheric pressure with a larger size of recirculation zone. Huang et al. [12] observed that the local Nusselt number on the whole of the target plate is dependent on the average jet $Re$ and that it increases with an increase in $Re$. A spent jet scheme wherein the spent air is allowed to exit in two-opposite directions performs better than the other spent jet schemes investigated as it yields the highest value of heat transfer coefficients on the target plate. Brevet et al. [13] pointed out that an optimum impinging distance for maximum performance would be in the range of $z/d$ = 2 to 5 and also suggested that a value of $z/d$ equal to 3 would be a worthy design consideration. Adimurthy and Katti [14] investigated experimentally the local distribution of wall static pressure and the heat transfer coefficient on a rough flat plate impinged

by a slot air jet. They observed that enhancement is found to decrease with the increase in the rib width. The results of the study can be used in optimizing the cooling system design, they also found that Wall static pressure coefficient decreases with increasing jet to plate distance due to entrainment of surrounding quiescent air. He and Wen [15] investigated experimentally the cooling performance of multiple impinging jets with different nozzle arrangements in a ground fast cooling simulation device. They proposed an overall performance evaluation indicator RU. RU ratio is flexible in weighing both the cooling rate and cooling uniformity. Based on the evaluation result, the N-4 nozzle arrangements prove to be the best when nozzle height H = 5 cm and H = 7.5 cm while the N-16 arrangement is optimum when H = 3.5 cm. They found Cooling performances of different nozzle arrangements vary a lot under different working conditions and are greatly dependent on air tank pressure and nozzle height conditions. An experimental investigation is carried out by Kumar et al [16] using slot jet with the parameter ranges from Reynolds number based on slot width is varied from 4200 to 12,000 and jet-to-plate spacing (*z/b*) is varied from 0.5 to 12. They identified three regions on plate namely They are stagnation region ($0 \leq x/b \leq 2$), transition region ($2 \leq x/b \leq 5$) and wall jet region ($x/b \geq 5$), and also found that For a particular z/b, increase in the Reynolds number increases the heat transfer coefficient at all the points in the stream-wise direction. Adimurthy and Katti [17] studied the local distribution of wall static pressure and heat transfer on a smooth flat plate impinged by a normal slot air jet. They varied parameters jet-to-plate spacing (*Z/Dh*) (0.5–10) and Reynolds number (2500–20,000) aspect ratio (*l/b*) of about 22. They found that Heat transfer coefficients are maximum at the stagnation point($x/Dh = 0$) for a given jet-to-plate distance and Reynolds number. Also, they observed that for the lower jet to plate distances and higher Reynolds number, secondary peaks are observed in the heat transfer distributions. These secondary peaks may be due to fluid transiting from laminar to turbulent flow on the target plate. However, the existence of secondary peaks is not prominent at the lower Reynolds number.

An experimental investigation is carried by Chambers et al.,[18] to determine the cross-flow effect of the jets cooling of a gas turbine blade. It was shown that initial crossflow strongly influenced the heat transfer performance with just 10 percent initial crossflow able to reduce the mean target plate jet effectiveness by 57 percent. Investigate experimentally to determine the effect of arrays of jets on various application is carried out by Geers et al., [19] they found that The measurements indicated that the interaction between the self-induced cross flow and the wall jets resulted in the formation of a system of horseshoe-type vortices that circumscribe the outer jets of the array. He et al.[20] Investigated experimentally the heat transfer characteristics of single-steady slot jet and synthetic slot impinging jets on a 25.4mm X 25.4mm vertical surface. The dynamic *Re* number was introduced to correlate heat transfer characteristics between synthetic jets and steady jets. Xing et al.[21] experimentally and numerically investigated the heat transfer characteristics within an array of impinging jets. The overall agreement of the results was very good and the local heat transfer coefficients were predicted at high accuracy.

A comprehensive review of turbulent flow characteristics of impinging jets and heat transfer is presented by Shukla and Dewan[22]. They observed that the majority of RANS based turbulence models did not predict impinging flows accurately and its complexities except a few. Many authors have reported that LES is capable of predicting the flow field and heat transfer data within the accepted accuracy limits. DNS can be applied to simple geometry with a low Reynolds number. Kanna et al.[23] Experimented on the cooling of an electronic device by thermosyphon method. In this method, they have used two-phase closed-loop thermosyphon to cool the electronic device under three working fluids (acetone, alcohol, and petrol). They found the maximum heat removal rate of about 65.4 % at 60 W is carried away by acetone in comparison with alcohol and petrol. This mainly because of the low boiling point and high latent heat of evaporation. Zeiny et al.[24] numerical analyzed the swirling effect of impinging jet on turbulent convective heat transfer over the hot plate containing obstacles. To create the swirling flow, a twisted tape was placed in the nozzle. They found that Nusselt number increases by 29 percent over the conventional impinging jet (CIJ) and in b/D=4, the heat transfer with the swirling flow would be more than CIJ.

Motevasel et al.[25] experimented to determine the heat transfer from Nano-fluids(Mgo/Water) nanofluids of various concentrations(0.02 to 0.12), and with different Reynolds number (11000 to 49000). It was found that at about 12 %, the heat transfer coefficient was increased compared with the base fluid. The complete review of discrete heated modules is carried out by Patil and Hotta [26]. The performace studies of the jet plate on solar collector is carried by Goel and Singh. [27]. They used the logitudinal fin arrengement to increses the perfoemce effect. They observed that the enhancement of 3–14.7% in thermal efficiency. also. Suhas et al [28]. They carried the numerical analysis on the different pipe bends at different curvature using micro and nano particle errsion. They observed that erosion depends mainly on Particle impact angle, Turbulence secondary flow. Mathew and Hotta [29] carried out the experimental and numerical studies on the cooling of the IC chips mounted on the SMPS board at different orientation. They found that $30^0$ will give temperature drop of 3-5% compared with horizontal orientation.

From the literature reviewed, it is observed that most of the work has been carried out with a single jet, But very few studies with the multiple jets with confinement effects are scarce. Their study considers two types of streamwise pitches of 2d, 4d at z/d =1.0 and 3.0 which result in local variations in wall static pressure coefficients. With an intention to partially fill the void in the literature reviewed, the following objectives were framed for the present study:

- To study the influence of nozzle-exit to target-plate spacing (*z/d*) on wall static pressure distribution ($C_p$) from impingement by an inline row of jets on a flat surface.
- To study the influence of spent air confinement on wall static pressure distribution ($C_p$) from impingement by an inline row of jets on a flat surface.
- To study the influence of streamwise pitch and cross-flow effect on wall static pressure coefficient ($C_p$) distribution under the impingement of multiple jets on a flat surface.

## 2. EXPERIMENTAL SETUP

### 2.1 Experimental Test rig

A schematic illustration of the experimental layout is shown in Fig. 1. The experimental work is carried out for different configurations to study the wall-static pressure distribution over a smooth flat plate under different spent air exit schemes, shown in Fig. 2. The experimental parameters are listed in Table 1. Air is supplied to the plenum chamber by a blower through a calibrated venturi meter. The plenum chamber having a cross-section of 200mm*100mm and length of 430mm made up of galvanized iron sheet houses three meshes or flow straighteners which serve the purpose of conditioning the fluid flow by removing any flow disturbances present in it. The volumetric discharge of air is regulated by a control valve located downstream of the venturi meter which subsequently sets up the required jet Reynolds number. An acrylic jet orifice plate (220mm*140mm*5mm thick) with an inline array of five orifice jets is fastened to the exit of the plenum chamber. The air via the supply channels, through the plenum chamber, exits the orifice plate in the form of five jets with high velocity and impinges on the target flat surface mounted on a 2-D traverse system. The 2-D traverse system also facilitates the setting up of the nozzle-exit to target-plate spacing.

The target plate (220mm*220mm*10mm thick) houses an acrylic strip, 10 mm thick, comprising of 0.5 mm pressure tap drilled into it for the length of 4 mm with its remainder of length being counter-bored for a diameter of 4 mm. The pressure-tap strip is free to move in the radial direction thereby facilitating the measurement of pressure distribution along the same. The experimental work involves constraining the spent-air exit to one side, two opposite sides, and all the four directions. The one-side and two-side spent-air exit schemes are achieved with the help of acrylic spacers glued on to the jet plates for three different nozzle-to-plate spacing ($z/d$'s).

### 2.2 Methodology

The air for the experimental study is supplied from a blower and the desired jet Reynolds number is set by setting the corresponding manometric deflection in the U-tube manometer connected to a calibrated venturi meter which is having Pipe diameter (d1) =25.4mm, Throat diameter (d0) =12.2mm, Beta ratio (β) =0.4815, Co-efficient of discharge (Cd) =0.9415 by carefully operating the flow regulating control valve. The venturi meter is designed in such a way that for all Reynolds number range studied the local fluid velocity is well below the local sonic velocity, i.e. the fluid flow Mach number is less than 0.3. Hence, air can be approximated as incompressible (constant density) fluid for all the parameters studied and subsequently a constant jet temperature throughout the supply channels leading to the orifice plate would be a fair assumption. Therefore, the jet air temperature is measured by employing a calibrated Chromel–Alumel Thermocouple (K-type) (Fig 1b) positioned at the inlet of the jets. The output of the thermocouple is measured by MECO millivoltmeter, Thermocouple placed upstream of the diffuser leading to the plenum chamber can be taken as the jet temperature at nozzle-exit. The stream-wise or radial Cp distribution over the target plate for all parameters and for all configurations is recorded with pressure tap housed in the movable strip which is part of the target plate with the pressure tap connected to a single column manometer via appropriate tube piping. The strip housing the pressure tap is moved in the radial or stream-wise direction in step lengths of 1mm to record the gauge wall-static pressure by reading the manometric deflection from the single column manometer.

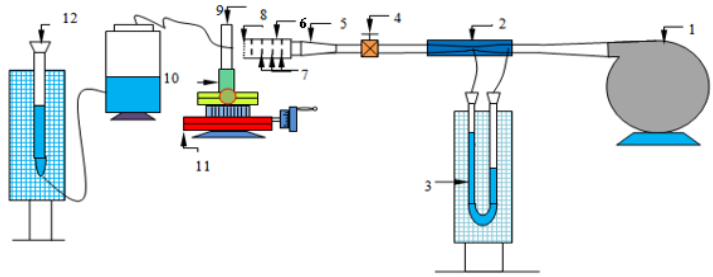


1) Air blower 2) Venturimeter 3) U-tube manometer 4) Control valve 5) Diffuser 6) Air plenum chamber 7) Flow straighteners (mesh-screens) 8) Jet plate 9) target plate 10) Support 11) 2-D Traverse system 12) Single water-column manometer.

**Figure 1**. Schematic illustration of the experimental layout.

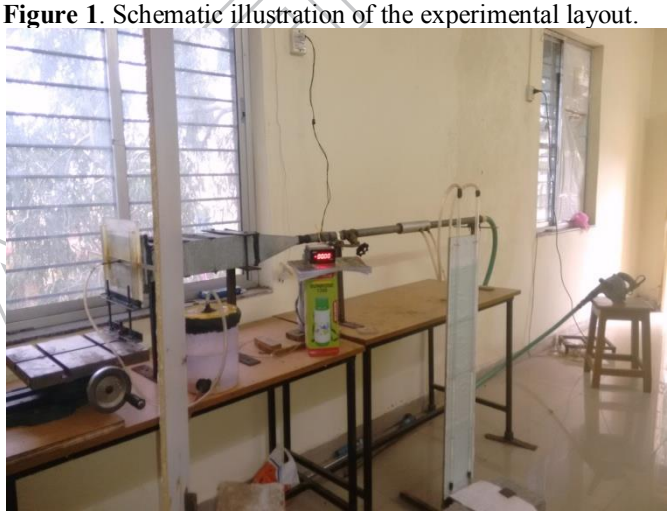

**Figure 1.a** Photographic view of Experimental test rig

**Table 1.** Experimental Parameters.

| | |
|---|---|
| Jet-diameter (d) | 5 mm |
| Nozzle exit to target plate spacing (z/d) | 1, 2 and 3 |
| Jet Reynolds number (Re) | 10000 |
| Jet length (l/d) | 1.0 |
| Stream-wise jet-to-jet spacing (s/d) | 2 and 4 |
| Number of jet orifices (n) | 5 |

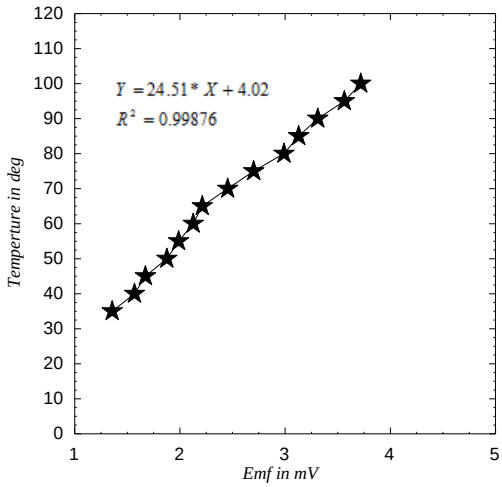


**Figure 1.**b Validation for K type Thermocouple

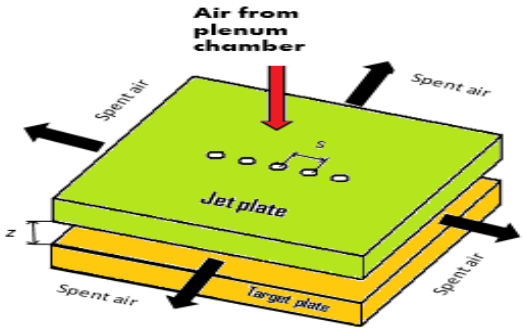


a) All side exit of spent air

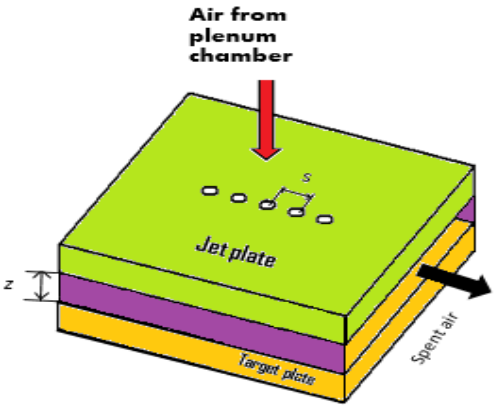


b) One side exit of spent air

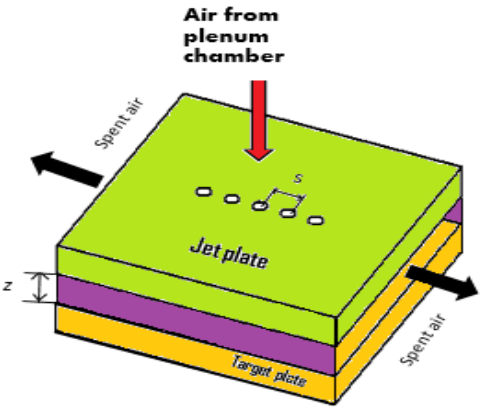


c) Two opposite side exit of spent air

**Figure 2.** Different spent air exit schemes

**2.3 Data reduction**

All the data reduction are standard which is used to calculate the discharge, velocity and head [14, 17]
Actual flow rate through venturimeter is given by,

$$Q_{act} = C_d \frac{a_1 a_2 \sqrt{2gH}}{\sqrt{a_1^2 - a_2^2}} \qquad (1)$$

$Q_{act}$ = actual flow rate of air ($m^3/s$); $C_d$ = coefficient of discharge; $a_1$ = cross sectional area at inlet section ($m^2$); $a_2$ = cross sectional area at throat section ($m^2$); g = acceleration due to gravity = 9.81 $m/s^2$

$$\text{H = equivalent head} = \left[\frac{\rho_w}{\rho_a} - 1\right] X \text{ , m}$$

$\rho_w$ = density of water ($kg/m^3$); $\rho_a$ = density of air ($kg/m^3$); X = manometer deflection (m)

Mean velocity of jet ($u_j$):

$$u_j = \frac{Q_{act}}{A_j} \qquad (2)$$

$A_j$ = cross section area of jet ($m^2$)
Jet Reynolds number (*Re*) based on nozzle diameter is given by:

$$\text{Re} = \frac{\rho u_j d}{\mu} \qquad (3)$$

$u_j$= mean velocity of jet (m/s); d = diameter of jet (m); μ= dynamic viscosity of air (pas or N-s/$m^2$)

Wall static pressure coefficient ($C_P$):

$$Cp = \frac{\Delta p}{0.5 \rho_a u_j^2} \qquad (4)$$

**2.3 Experimental Uncertainty**

The uncertainty in the primary quantities has been obtained by calibration of the instruments, and for derived quantities it has been calculated, based on the uncertainty of primary quantities Venkateshan S P [30], and is shown in Table 2 The ISO guide has been followed for the calculation of uncertainty of derived quantities, as given in Kessel W [31]. The uncertainty in the $C_P$ measurement is 2.7% at Reynolds number 10000. The formula for calculation of uncertainty is given in Eq 5

$$\Delta\sigma = \pm\sqrt{\sum_{i=1}^{N} \left(\frac{\partial \sigma}{\partial m_i} \times \Delta m_i\right)^2} \qquad (5)$$

**Table 2. Uncertainty Physical quantity**

| Sl No | Physical quantity | % Uncertainty |
|---|---|---|
| 1 | Temperature | ±0.5% |

| | | |
|---|---|---|
| 2 | Flow rate | ±1.2% |
| 3 | Displacement | ±1% |

## 3. RESULTS AND DISCUSSION

### 3.1 Influence of z/d and spent air confinement on the distribution of wall-static pressure coefficient ($C_p$) over a flat surface at s/d of 2

Fig. 3 shows the variation in the distribution of wall-static pressure coefficient with the change in nozzle-exit to target-plate spacing (*z/d*) over a flat smooth surface at *s/d* of 2 for three different spent air exit schemes. As can be seen in Fig. 3. for all *z/d*'s studied, the maximum in $C_p$ occurs at all stagnation points on the target surface and the $C_p$ value decreases with the increase in the radial distance (*r/*s) from the respective stagnation points of each of the five jets. Inferring from the Fig 3b and 3c, the jets down-stream before impinging on the surface are deflected by incoming flow of the spent air upstream to them in the direction of the crossflow.

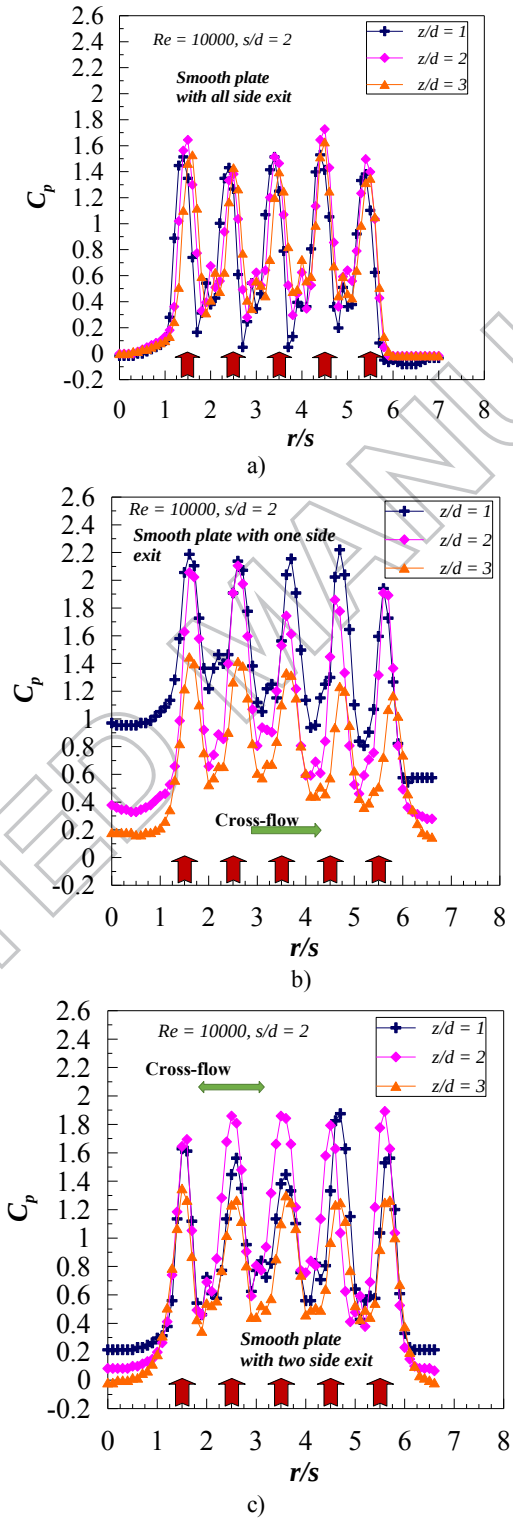


**Figure 3.** Influence of *z/d* on the distribution of wall-static pressure coefficient ($C_p$) over a flat surface at *s/d* of *2* with spent air constrained to exit from: a) all sides, b) one side, c) two opposite sides

The shift in stagnation point $C_p$ increases with the decrease in *z/d* and shifts away from their respective geometric centers in the direction of the spent air cross-flow. Also in Fig. 3., a secondary peak in the value of $C_p$ can be seen for all *z/d*'s, the location of which is approximately in between the two adjacent stagnation points. These secondary peaks in $C_p$ are attributed to the formation of fountains or up-wash on the target surface, the formation of which in turn is attributed to the collision of the neighboring wall-jets as they move out in a direction tangential to the target surface after their impingement on it. These secondary peaks also suffer a deflection as that of the primary peaks in the direction of the cross-flow. There exists a minimum value of $C_p$ between two consecutive stagnation points. The magnitude of these minimum $C_p$'s: "increases with increase in *z/d* for the case with all sides exit scheme, decreases with increase in *z/d* for the case with one side exit and remains more or less the same for the case with two side exit scheme", as seen in Fig. 3. These minimum $C_p$'s also suffer deflection in the direction of the spent jet flow corresponding to the deflection in primary peaks.

The influence of nozzle-exit to target-plate spacing (*z/d*) on the $C_p$ distribution is more pronounced in cases where there is appreciable confinement of the spent air exit flow, seen in Fig. 3b (spent air exit from one side) and Fig. 3c (spent air exit from two opposite sides) compared to Fig. 3a where *z/d* has a negligible influence on the $C_p$ distribution, as the spent air is allowed to exit in all directions. This is perhaps because of the cross-flow effect of spent air, which increases with the increase in the confinement of spent air exit flow. As can be seen in Fig. 3b, here the spent air is allowed to exit in one direction, the value of $C_p$ at all radial locations (*r/s*) decreases as *z/d* increases. This is probably because the amount of air flowing across the main jet flow direction i.e. the cross-flow effect increases with increase in z/d and subsequently more of the jet's momentum is carried away by the spent air, as can be inferred from corresponding drop in the value of $C_p$ and subsequently the jets also suffers a deflection from their respective geometric centers. Also in Fig. 3b, for *z/d* = 3 there is a monotonic decrease in the value of stagnation point Cp unlike in the case of *z/d* = 1 & 2 as you move downstream in the direction of the spent jet flow. This is because the jets downstream have to face more and more accumulated spent air of the jets upstream to them, therefore the jet which is far downstream suffering a maximum drop in the value of $C_p$ as it encounters the maximum amount of accumulated spent air.

### 3.2 Influence of z/d and spent air confinement on the distribution of wall-static pressure coefficient ($C_p$) over a flat surface at s/d of 4

Fig. 4 shows the variation in the distribution of the wall-static pressure coefficient with a change in nozzle-to-plate spacing (z/d) over a flat surface at a stream-wise jet-to-jet spacing of 4d for three different spent air exit schemes. As can be seen in Fig. 4., for all *z/d*'s studied, the maximum in $C_p$ occurs at all stagnation points on the target surface and the $C_p$ value decreases with the increase in the radial distance (*r/s*) from the respective stagnation points of each of the five jets. Inferring from the Fig 4b, the jets downstream before impinging on the surface are deflected by incoming cross-flow of spent air from the jets upstream to them in the direction of the cross-flow. These shifts in stagnation point $C_p$ increases with an increase in *z/d* and they have deflected away from their respective geometric centers in the direction of the spent air cross-flow. However, referring to Fig. 4c, the shift in the stagnation point $C_p$' are not as pronounced (relatively less) in the case where the spent air is allowed to exit from two opposite directions in comparison to the case wherein the spent air is allowed to exit in one direction only. This is because in the latter case the spent air has a longer path to travel and as it travels downstream, the cross-flow associated with it only becomes stronger and stronger which is unlike in the former's case where spent air has to travel a lesser path to escape out and subsequently having relatively lesser cross-flow effect. Also, referring to Fig. 4b and 4c, the stagnation point $C_p$'s decrease as z/d increases. This could be because the amount of accumulated spent air flowing across the direction of impinging jets increases with an increase in *z/d*. Inferring from Fig. 4, out of all the spent air schemes studied the strongest cross-flow effect can be seen in the case where the spent air is constrained to escape out from one side only as the jets are seen to undergo maximum shifts in their stagnation points relative to their respective geometric centers. The *z/d* has a minimum effect on the $C_p$ distribution for the case with all sides exit scheme, the medium effect on $C_p$ distribution for the case with two opposite sides exit scheme and maximum effect on $C_p$ distribution for the case with one side exit scheme.

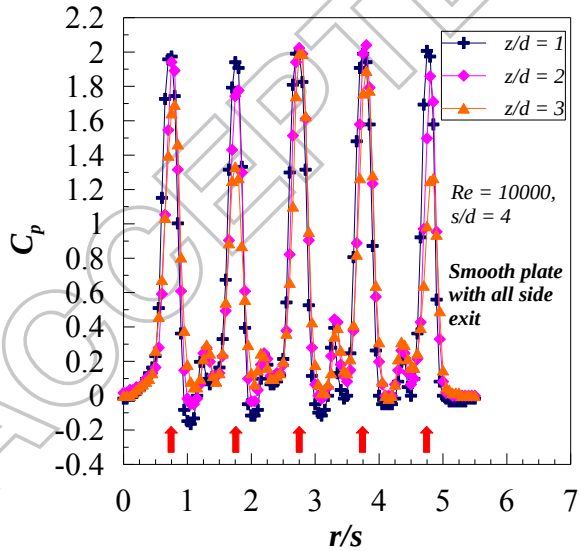


a)

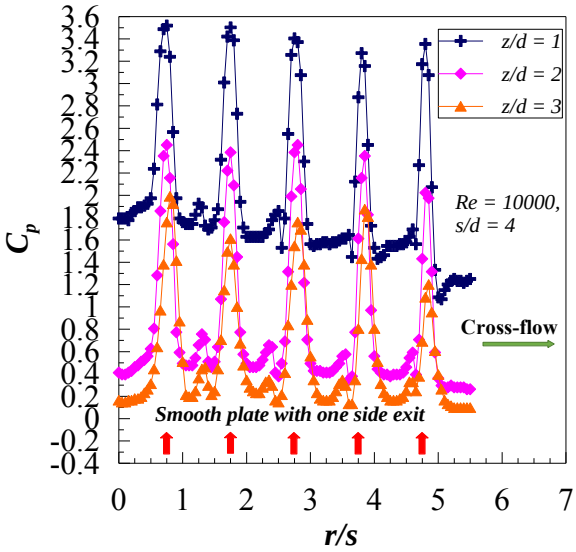


b)

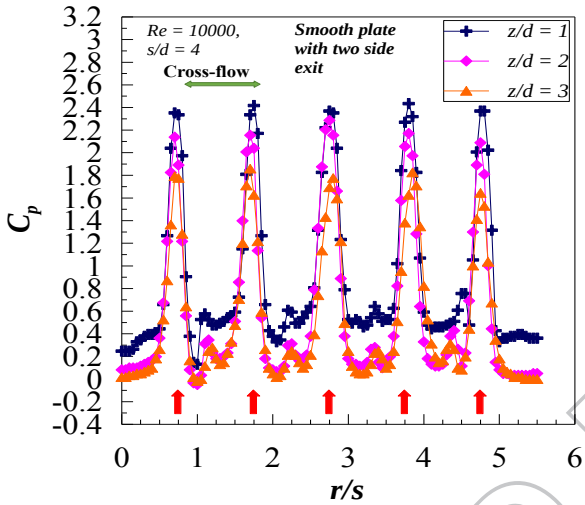


c)

**Figure 4**. Influence of *z/d* on the distribution of wall static pressure co-efficient With spent air constrained ($C_p$) over a flat surface at s/d of 4d to exit from a) all sides, b) one side, c) two opposite sides

**3.3 Influence of *s/d* on the distribution of wall-static pressure coefficient ($C_p$) at different *z/d* over a flat smooth surface with spent air exit from all directions.**

Fig 5 shows the effect of *s/d* on the distribution of wall-static pressure coefficient ($C_p$) over a flat smooth surface with spent air exit from all directions at different *z/d*'s. As can be seen in the figure 4.7*a*, 4.7*b* and 4.7*c*, for all *z/d*'s studied and both *s/d* of 2 as well as 4, the maximum in $C_p$ occurs at all stagnation points on the target surface and the $C_p$ value decreases with the increase in the *r/s* from the respective stagnation points of each of the five jets and reaches a value of zero (i.e. atmospheric pressure) at sufficient distance from centers of the jets at the extreme ends.

Referring figures 5.*a*, 5.*b* and 5.*c*, it is seen that the $C_p$ distribution over the flat smooth surface is a function of *s/d*. The stagnation points $C_p$ of all the five jets increase with the increase in *s/d* for all *z/d*'s studied. Also from figure 5, it can be noted that the value of secondary peaks in $C_p$ decreases with the increase in the *s/d* for all *z/d*'s studied. This perhaps has to do with the fact that, jets after impinging and then turning tangential to the target surface i.e., wall jets have a longer distance to travel before they collide with each other on the target giving rise to secondary peaks. The wall jets lose more momentum with the distance traveled.

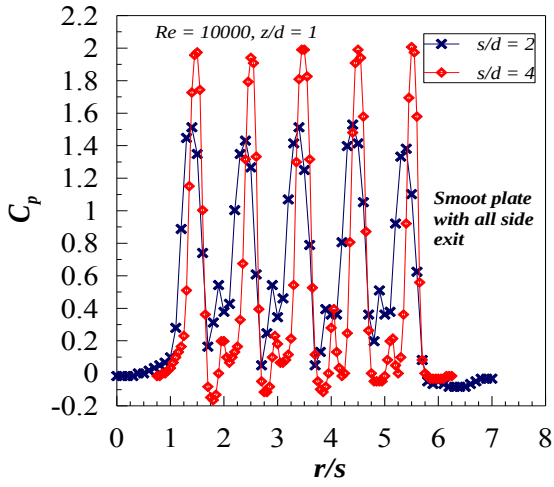


a)

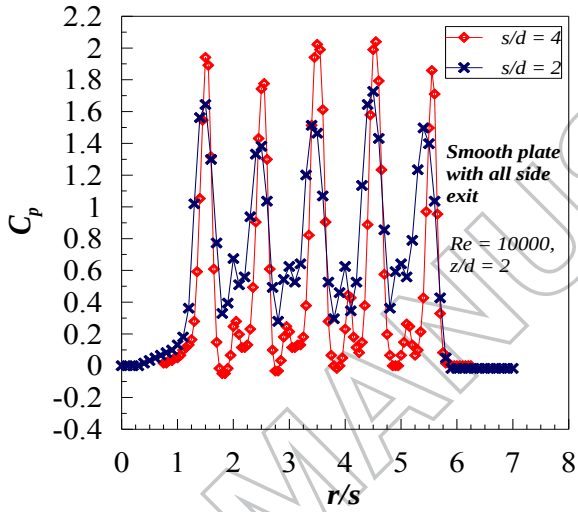


b)

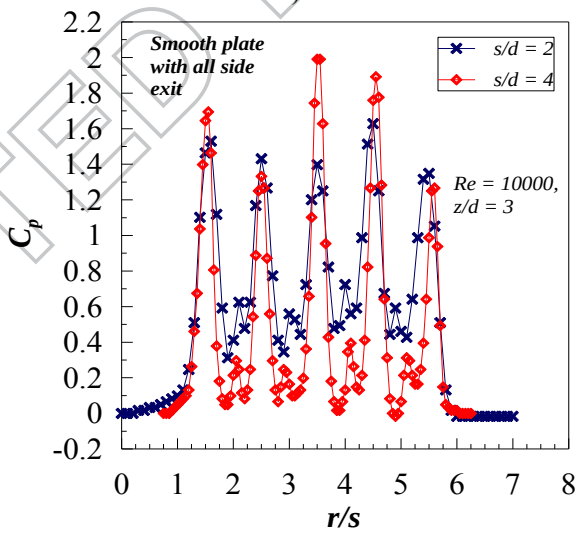


c)

**Figure.5** Effect of *s/d* on $C_p$distributionover a flat smooth surface with spent air exit from all directions at; a) *z/d = 1*, b) *z/d = 2*, c) *z/d = 3*

As the distance wall jets have to travel and subsequently the momentum they lose before their collision is directly proportional to the stream-wise jet-to-jet spacing, the values of secondary peaks in $C_p$ are less at a jet-to-jet spacing of *4d* than that at *2d*.

## 4. CONCLUSIONS

The conclusions from the present experimental study are as summarized below:

- The maximum wall-static pressure coefficient ($C_p$) occurs at stagnation points of all the five jets corresponding to their respective geometric centers over the flat plate at all *z/d*'s studied when the spent air is allowed to escape out from all directions while it occurs slightly off their geometric centers when the spent air is constrained to escape out from one and two opposite directions.
- Secondary peaks in $C_p$ as a consequence of the collision of wall jets over the target surface are seen approximately between two successive stagnation points for all *z/d*'s studied and are deflected in the direction of the spent airflow for the cases where the spent jet is constrained to exit from one and two opposite directions.
- There is a gradual decrease in the value of $C_p$ from closed-end to exit end when spent air exits from one direction owing to the crossflow effect i.e., the jets downstream have to face more and more accumulated spent air from their upstream counterparts.

**REFERENCES**


[1] Katti, V, V., Prabhu, S, V., 2009 "Influence of streamwise pitch on the local heat transfer characteristics for in-line arrays of circular jets with crossflow of spent air in one direction," Heat Mass Transf. 45 (9), 1167–1184

[2] Wolf, W., Koller, W, D., Spieu, W, E, L., 1999 "Impinging jet drying of pressed fish cake," J. food. Engg 40, 113–120.

[3] Chang,, W., Chiou, S., F., Chang,, S, F., 2007 "Heat transfer of impinging jet array over a concave-dimpled surface with applications to cooling of electronic chipsets," Exp. Therm. Fluid Sci., 31(7), 625–640.

[4] N. Karwa, 2012 "Experimental Study of Water Jet Impingement Cooling of Hot Steel Plates," PhD.Thesis.

[5] Wadsworth, D., Mudawar, I., 1989 "Cooling of a multichip electronic module by means of confined two-dimensional jets of dielectric liquid," J. Heat Transf., 112, ,891-898.

[6] Hotta, T, K., Muvvala, P., Venkateshan, S, P., 2013 "Effect of surface radiation heat transfer on the optimal distribution of discrete heat sources under natural convection," Heat Mass Transf, 49(2), 207–217.

[7] G. Casano and S. Piva, 2015 "Air-Water Cooling System for Switch-Mode Power Supplies," J. Electro Cooling Thermal Contr, 5, 66–75.

[8] Gardon, R., Cobonpue J 1962 "Heat transfer between a flat plate and jets of air impinging on it", International developments in heat transfer. In: Proceedings of 2nd international heat transfer conference. ASME, 454–460

[9] Gardon R. Akfirat C 1966 "Heat Transfer characteristics of impinging two-dimensional air jet" J.Heat Transf 88 101-108.

[10] Viskanta R. 1993 "Heat Transfer to Impinging Isothermal Gas and Flame Jets, Experimental Thermal and Fluid Science, 11-134

[11] Colucci D. W. Viskanta R 1996 "Effect of Nozzle Geometry on Local Convective Heat Transfer to a Confined Impinging Air Jet", International Journal of Experimental Thermal and Fluid Science, 13 71-80.

[12] Huang Y, Ekkad S V, Han Je-Chin. 1998 "Detailed Heat Transfer Distributions under an Array of Orthogonal Impinging Jets", J. Therm physi Heat Transfer.12(1), 73–79

[13] Brevet P, Dejeu C, Dorignac E, Jolly M, Vullierme J J 2002 "Heat Transfer to a Row of Impinging Jets in Consideration of Optimization" Int. J. Heat Mass Transf .45(20) 4191–4200

[14] Adimurthy M, Katti, V "Local distribution of wall static pressure and heat transfer on a rough flat plate impinged by a slot air jet" Heat Mass Transf.53, 2497-2515

[15] He, Y, L., Wen, Z, X., 2017 "Experimental study on cooling performance of multiple impinging jets with different nozzle arrangements in a ground fast cooling simulation device Appl Therm Engg. 113, 1024-1032.

[16] Kumar N M, Katti V V, Prabhu S V 2011 "Local heat transfer distribution on a smooth flat plate impinged by slot jet" Int. J. Heat Mass Transf.54 727-738

[17] Adimurthy M, Katti, V, V., 2017 "Local distribution of wall static pressure and heat transfer on a smooth flat plate impinged by a slot air jet" Heat Mass Transf 53, 2497-2515.

[18] Chambers, A., Gillespi, D., Ireland, P., Dailey, G., 2005 "The Effect of Initial Cross Flow on the Cooling Performance of a Narrow Impingement Channel", J. Heat Transfer. 127 358-365.

[19] Geers, L, F, G., Tummers, M, J., Hanjalić, H., 2004 "Experimental investigation of impinging jet arrays" Exp. Fluids. 36, 946–958.

[20] He, X, Lustbader, A, J., Arik, M., Sharm, R., 2015 "Heat transfer characteristics of impinging steady and synthetic jets over the vertical flat surface", Int. J. Heat Mass Transf. 80, 825–834.

[21] Xing,, Y., Spring,, S., Weigand, B., 2010 "Experimental and Numerical Investigation of Heat Transfer Characteristics of Inline and Staggered Arrays of Impinging Jets", J. Heat Transfer. 132 , 92201-11.

[22] Shukla, A.., Dewan A., 2017 "Flow and thermal characteristics of jet impingement: two-dimensional comprehensive review" Int. J. Heat Technol. 35, 153–166.

[23] Kannan K, G., Kamatchi, R., Venkatajalapathi K, Krishnan, A, S., 2018 "Enhanced heat transfer by thermosyphon method in electronic devices", Int. J. Heat Technol. 36, 339–343.

[24] Zeiny, E., Farhadi, M., Sedighi, K., 2017 "Numerical investigation of the simultaneous influence of swirling flow and obstacles on a plate in impinging jet" Int. J. Heat Technol. 35, 59–66.

[25] Motevasel, M., Nazar, A, R, S., Jamialahmadi, M., 2017 "Experimental investigation of turbulent flow convection heat transfer of MgO/water nanofluid at low concentrations - Prediction of aggregation effect of nanoparticles", Int. J. Heat Technol. 35, 755–764.

[26] Patil, N, G., Hotta, T, K., 2018 "A review on the cooling of discrete heated modules using liquid jet impingement" Front. Heat Mass Transf. 11 2018.

[27] Goel, K, A., and singh N., 2017 "Performance studies of a jet plate solar air heater with longitudinal fins" Int. J, Ambt, Enrgy., 1-9.

[28] Shinde, S, M., Kawadekar, D, M., Patil, P, A., Bhojwani, V, K., 2019 "Analysis of micro and nano particle erosion by the numerical method at different pipe bends and radius of curvature" Int. J, Ambt, Enrgy., 1-9.

[29] Mathew, V, K., Hotta T, K., 2020 "Experiment and Numerical investigation on optimal distribution of discrete ICs for different orientation of substrate board" Int. J, Ambt, Enrgy., 1-9

[30] Venkateshan SP 2008 Mechanical measurements. Ane Books, New Delhi

[31] Kessel W 2002 Measurement uncertainty according to ISO/ BIPM-GUM. Thermochimica Acta 382(1):1–16

**NOMENCLATURE**

$A_j$ Cross-section area of the jet, $m^2$

$C_p$ Wall static pressure coefficient, $Cp = \frac{\Delta p}{0.5 \rho_a u_j^2}$

d Diameter of the jet, m

l/d Non-dimensional length of the jets

r/s Non-dimensional radial distance

Re Reynolds number, $\mathrm{Re} = \frac{\rho u_j d}{\mu}$

$u_j$ mean velocity of the jet, m/s

s/d Non-dimensional streamwise jet-jet spacing

z Distance between nozzle exit plane and target plate plane

z/d Non-dimensional distance between nozzle exit plane and target plate plane

**Greek symbols**

μ Dynamic viscosity of air (pas or N-s/$m^2$)

**ρ** Density kg/$m^3$